Gelatin–Graphene Nanocomposites with Ultralow Electrical Percolation Threshold

Hoda Nassira, Antoni Sánchez-Ferrer, Jozef Adamcik, Stephan Handschin, Hossein Mahdavi, Nader Taheri Qazvini, and Raffaele Mezzenga**

Recent advances in bio-nanotechnology have increased the demand for conductive biopolymer nanocomposites (CPCs).[1] CPCs are obtained by structuring a network of conductive nanofillers (carbon allotropes or metallic-based nanoparticles) embedded into an insulating biopolymer matrix. However, high loading levels of conductive particles are generally needed in order to achieve electrical percolation, and the technical difficulties associated with the surface functionalization of these particles[2–6] severely limit the applicability of CPCs. Therefore, formulating new CPCs with lower electrical percolation threshold, which require properly dispersing the conductive nanoparticles, constitutes a topic of great importance. This is particularly true in the case of graphene-based biopolymer nanocomposites, where the hydrophobic nature of graphene represents a heavy drawback when water-processed biopolymers must be used. The introduction of graphene-based compounds into biopolymer matrices has been an important strategy for the modification of the mechanical, electrical, and functional properties of these polymers while maintaining their biocompatibility.[2,7,8]

As a structural protein, gelatin is an unexplored promising candidate in preparing graphene-based CPCs with low percolation threshold in which the excellent conductivity of graphene combines with the biodegradability and biocompatibility of gelatin.

Gelatin has been used in applications ranging from photographic paper coatings to food processing due to its unique rheological properties, non-toxicity, non-immunogenicity, low price, and high water sensitivity.[9–11] Furthermore, biodegradability and biocompatibility of gelatin make it a promising material for applications such as wound dressings,[12–14] controlled drug delivery systems,[15,16] bone scaffolds,[16,17] and arterial implants.[18]

In order to exploit the superior physical properties of graphene at best, homogeneous dispersions into the gelatin matrix and an effective interfacial stress-transfer between the graphene nanosheets and polymer matrix are required. To overcome the hydrophobic nature of graphene and make it biocompatible, biofunctionalization based on noncovalent interactions has been thoughtfully explored.[19–22] Nonetheless, the proposed approaches usually rely on very expensive precursors and/or do not entirely preserve the electrical and physical properties of graphene.[19–22] Therefore, owing to the more hydrophilic nature of the graphene oxide (GO) surface, which allows more affordable dispersions in aqueous media, GO has been usually preferred over graphene,[23] specially in bio-related applications.[24] For example, GO dispersed in functionalized or neat gelatin matrix has found applications in tissue engineering and drug delivery.[25,26] Moreover, it was found that gelatin can help the exfoliation of naturally occurring graphite in aqueous media or to be a reducing agent for GO.[27–29] However, the residual gelatin chains on the basal plane of graphene generally impeded the required electron and phonon transfer,[27,28] and the conductivity of such nanocomposites from this type of graphene has never been reported.[29,30] In this regard, using less amount of gelatin as adhesive in GO film led to conductive graphene-based nacre after reduction in hydroiodic acid.[31] Nevertheless, all of the above reported techniques suffer from one main problem: loss of electrical conductivity at the expense of dispersibility of graphene nanosheets in water. In other words, a compromise between good processability in water and preservation of conductivity is still highly pursued and constitutes the main topic of active scientific efforts.

Here, we propose an environmentally friendly and inexpensive approach to this problem. Taking advantage of the electrostatic interactions between gelatin and GO, the sp^2 carbon orbital configuration of graphene is restored by the synergistic action of gelatin and ascorbic acid (Vitamin C) as reducing agents[27,32] after reducing in situ the surface of GO nanosheets embedded in the gelatin matrix, leading to an unprecedented low percolation threshold of the graphene nanosheets.

Gelatin–graphene nanocomposites were prepared by mixing gelatin and GO dispersions, and by further reduction of GO in the presence of ascorbic acid - a natural antioxidant and a well-known bio-reducing agent[32,33] (**Scheme 1**).

To study the quality of the dispersion prior to casting, atomic force microscopy (AFM) was employed to resolve the morphology of individual nanosheets (**Figure 1**a). The measured thickness of the flat GO single nanosheet is ≈1 nm,

H. Nassira, Dr. A. Sánchez-Ferrer, Dr. J. Adamcik, S. Handchin, Prof. R. Mezzenga
ETH Zurich
Department of Health Sciences and Technology
Food and Soft Materials Science
IFNH
Schmelzbergstrasse 9, 8092 Zürich, Switzerland
E-mail: raffaele.mezzenga@hest.ethz.ch
H. Nassira, Prof. H. Mahdavi, Dr. N. Taheri Qazvini
Polymer Division
School of Chemistry
College of Science
University of Tehran
P.O. Box 14155-6455, Tehran, Iran
E-mail: ntaheri@ut.ac.ir
Dr. N. Taheri Qazvini
Institute for Molecular Engineering
University of Chicago
Chicago, IL 60637, USA

DOI: 10.1002/adma.201601115

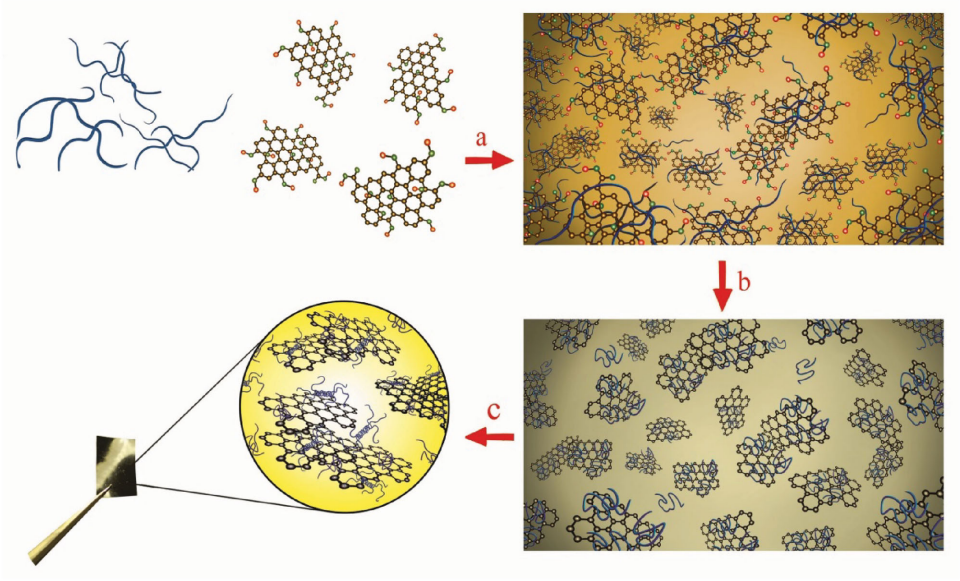

Scheme 1. Schematic for the fabrication of free-standing gelatin–graphene nanocomposite films. a) Ionic interaction between negatively charged GO and positively charged gelatin chains. b) In situ reduction of GO at 95 °C in the presence of ascorbic acid (not shown here) and gelatin under vigorous stirring. c) Mixing of the obtained gelatin/graphene dispersion with extra gelatin in order to obtain the desired graphene concentration, and solvent casting of the films.

confirming exfoliation of the nanosheets (Figure 1a). The GO nanosheet precursor is negatively charged in the pH range from 2 to 10 (Figure 1b), while the net surface charge of gelatin switches from positive to negative beyond the isoelectric point at pH 5.2 (Figure 1b). Thus, the strongest attractive electrostatic interaction between the GO nanosheets and gelatin occurs at pH 3.0, where the associative interactions between the positively charged amino acids and the negative charges on GO nanosheets lead to the formation of a complex between the two components (Scheme 1a). GO was reduced

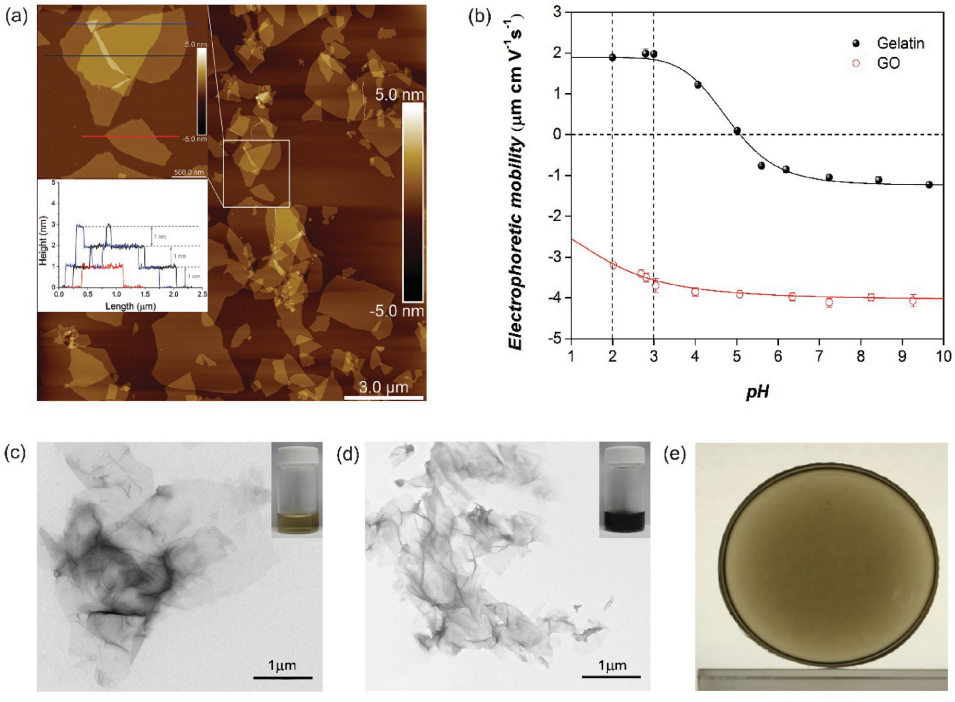

Figure 1. Interaction of GO and graphene with gelatin chains. a) AFM images of GO with the corresponding height profiles (inset). b) Electrophoretic mobility of gelatin and GO dispersion in pure water as a function of pH. c) TEM images of gelatin/GO dispersion. d) gelatin/graphene dispersion. e) Optical image of gelatin/graphene nanocomposite (filler concentration is 0.09 wt%).

to graphene by stirring the suspension of gelatin/GO at pH 3.0 and adding ascorbic acid at 95 °C for 1 h (Scheme 1b). It should be noted that since the complexation between gelatin and GO is altered by pH variations, the reducing agent should not change the pH of the media. Contrary to the most common reducing agent, i.e., hydrazine, ascorbic acid does not significantly change the pH, which remains in the range of 2.9 ± 0.2 over the period of the reduction process, which is ideal for electrostatic interactions, as these are maximized in the pH range of 2–3.

The resulting gelatin/graphene dispersion was further mixed with gelatin in order to obtain the desired composition of graphene in the mixture. Finally, films were obtained by solvent casting (Scheme 1c).

Reduction of GO with ascorbic acid alone, under the same conditions, was not stable and the system precipitated due to strong π–π stacking and hydrophobic interactions. Thus, gelatin was instrumental for dispersing the resulting reduced graphene oxide. In order to directly observe the dispersion of graphene nanosheets into the gelatin matrix, transmission electron microscopy (TEM) imaging was carried out on the nanocomposite dispersion before and after the reduction (Figure 1c,d). The GO nanosheets were uniformly dispersed in the gelatin dispersion (Figure 1c). After reduction, the wrinkled graphene nanosheets remained dispersed and no aggregation was observed (Figure 1d). TEM imaging on samples containing 1, 10, and 15 wt% graphene showed comparable dispersibility before and after the reduction (Figure S1, Supporting Information). Optical images of the final nanocomposite films reflect the dispersion quality for the sample containing 0.09 wt% graphene (Figure 1e) as well as the samples with higher concentrations of graphene (Figure S2, Supporting Information).

Besides, AFM images (**Figure 2**a–c) prove that gelatin chains were selectively adsorbed on the graphene surface before and after the reduction, as indicated by the thickness of the single GO and graphene nanosheets of ≈5 nm (Figure 2c). Moreover, gelatin prevented the aggregation of the graphene nanosheets during the reduction process. Control experiments showed that reduction of GO in the absence of gelatin resulted in aggregation of graphene nanosheets. Furthermore, films obtained in the absence of ascorbic acid showed very low conductivity (Table S1, Supporting Information).

In order to confirm the presence of graphene–gelatin complexes, the carbon structure of the nanocomposites was characterized by Raman spectroscopy (Figure 2d). The characteristic Raman bands of carbon-based sp^2 materials are found around 1350, 1580, 2700, and 2900 cm^{-1}, and are attributed to D, G, 2D, and D′ bands, respectively. The D band is assigned to structural disorders, while the G band is related to the E_{2g} phonon of sp^2 carbon atoms.[34] The peak intensity ratio of the D and G bands (I_D/I_G) is proportional to the average size of the sp^2 domains.[35,36] This intensity ratio is also used to estimate the degree of order in crystalline structures of graphene. The I_D/I_G of gelatin/GO (1.1) and gelatin/graphene (1.06) slightly increased in comparison with that of pure GO (0.97), indicating a very small decrease in the mean size of the sp^2 domains. This indicates that noncovalent functionalization of the carbon basal plane in the presence of gelatin and ascorbic acid is an effective approach for the obtaining of graphene nanosheets. Moreover, while the D and G peak positions of both GO and gelatin/GO are identical, the G band positioning of gelatin/graphene gradually shifted to 1587 cm^{-1} – similar to that of natural graphite (1581 cm^{-1}). This Raman shift of the G band indicates the presence of single and double layer crystal structure of graphene in the as-prepared gelatin/graphene nanocomposite.[37] Furthermore, the shape and the shift of the 2D band in the gelatin/graphene material to values lower than 2700 cm^{-1} could be attributed to the presence of isolated layers,[38] as confirmed by the AFM height profile of gelatin/GO and gelatin/graphene systems (Figure 2a–c).

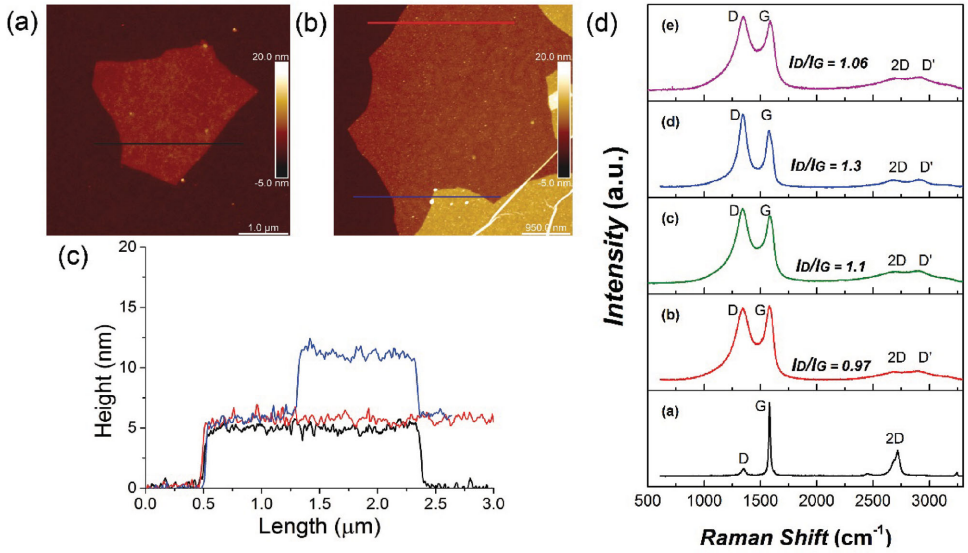

Figure 2. Surface characterization of gelatin/graphene dispersion and nancomposite. a) AFM images for the gelatin/GO dispersion before reduction. b) AFM images for the gelatin/graphene dispersion after reduction of the GO. c) Corresponding height profiles collected along the AFM images before (black) and after reduction (blue and red). d) Raman spectra of: a) graphite, b) GO, c) gelatin/GO nanocomposite, d) graphene, and e) gelatin/graphene nanocomposite (filler concentration in nanocomposite is 10 wt%).

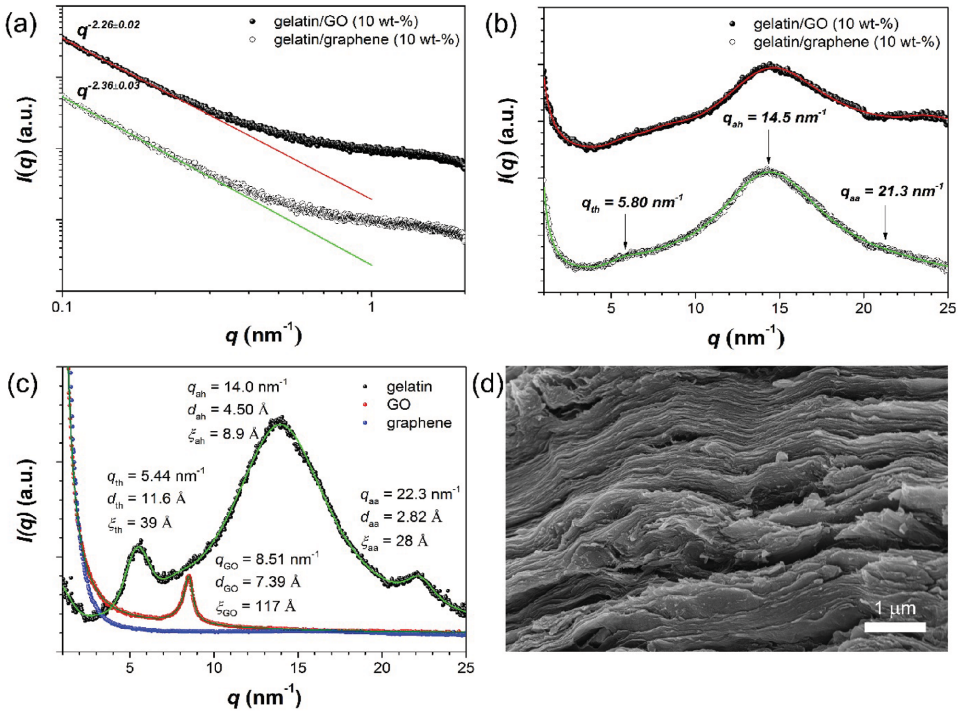

Figure 3. Structural characterization of free-standing gelatin/graphene nanocomposite films. a) 1D SAXS intensity profile; the red and green lines are the slopes at low q values for the gelatin/GO and gelatin/graphene nanocomposites. b) 1D WAXS intensity profile for the gelatin/GO and gelatin/graphene nanocomposites; the red and green curves are the fit to the WAXS profile for the different nanocomposites. c) 1D WAXS intensity profile for the pure gelatin (black circles), graphene oxide GO (red circles), and graphene (blue circles); the green and red curves are the fits to the gelatin and GO WAXS profiles, respectively. d) SEM images of the nanocomposites (filler concentration in nanocomposite is 10 wt%).

Small- and wide-angle X-ray scattering (SAXS and WAXS) were used in order to study nonintrusively the conformation of nanosheets within the polymer matrix. The intensity at low q values (SAXS) is dominated by the scattering of objects in the 1–100 nm range, and therefore can be used to probe the dispersion state of graphene in the nanocomposites (**Figure 3**a). On the other hand, the intensity at high q values (WAXS) is related to the sub-nanometer scale where the gelatin–gelatin distance is visible (Figure 3b). The slope of the SAXS scattering intensity profile at very low q values gives information about the fractal dimensionality of the objects dispersed into the polymer matrix, i.e., the scattered intensity scales with the scattering vector as $I(q) \propto 1/q^m$.[39] 2D objects show a slope value of $m = 2$, while aggregates or 3D objects approach values of $m = 3$ or higher. The slopes observed for the gelatin/GO and gelatin/graphene nanocomposites are 2.26 and 2.36, respectively (Figure 3a), which indicate an almost perfect dispersion of isolated graphene nanosheets in the samples, especially bearing in mind the relatively high concentration (10 wt%) used to collect the scattering profiles. Importantly, reduction with ascorbic acid does not alter the orientation and uniform dispersion of graphene nanosheets in the nanocomposites. The deviation of the fractal dimension from the ideal value of 2, beyond the high graphene content in these samples, can be explained based on the fact that the exfoliated graphene-based materials are often compliant, and they typically bend or crease when dispersed in a polymer matrix.[40] The affinity between the nanosheets and the polymer matrix has been reported to affect this conformational change of the graphene-based materials. The stronger is the interaction between the graphene nanosheets and the polymer matrix, the more extended is the conformation of the nanoobject.[41] Moreover, the technique used to prepare the nanocomposites can alter the microstructure and the orientation of the nanosheets. Solution mixing usually favors random orientation and exfoliation of the nanosheets, while the samples processed by melt mixing are more likely to contain stacked structures.[42]

The WAXS intensity profiles (Figure 3b) were similar to that of pure gelatin (Figure 3c), which shows three peaks, at q = 5.44, 14.0, and 22.3 nm^{-1}, corresponding to the characteristic distances of 11.6 (interhelical distance), 4.5 (intergelatin distance), and 2.8 Å (translation per triple helical triplet), respectively.[43] In addition to the broad scattering peak at q = 14.5 nm^{-1} (d = 4.3 Å) for the nanocomposites, ad low-intensity broad peak at q = 5.8 nm^{-1} (d = 1.08 nm) was observed. This WAXS intensity profile for the gelatin nanocomposites indicates that the helical secondary structure expected for gelatin was still occurring even in the presence of GO or graphene in the gelatin matrix. In particular, the WAXS analysis illustrates the strong electrostatic interaction between gelatin and GO, which led to a decreased content of helical secondary structures. Highly aligned GO nanosheets dispersed in gelatin may have directed the orientation of the ionic domains of gelatin chains. In support of this hypothesis, the helical content of gelatin increased after reduction (Figure 3b) indicating the release of strong electrostatic interactions, with the remaining

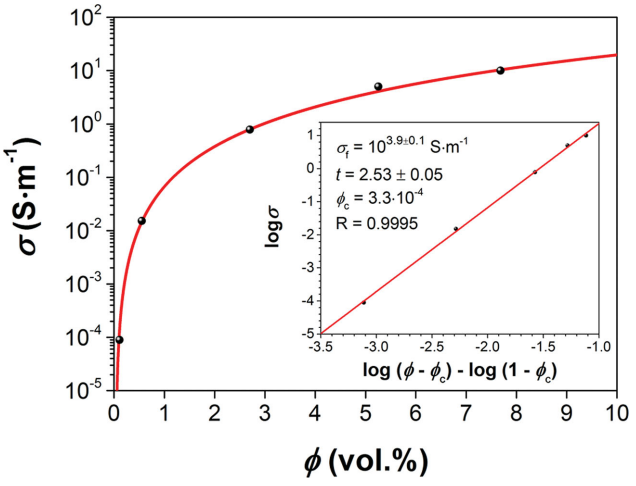

Figure 4. Electrical conductivity σ for the different gelatin/graphene nanocomposites as a function of the graphene volume percentage. The red curve is the fit to the data using the percolation model. The inset is the log–log plot of σ versus $(\phi - \phi_c)/(1 - \phi_c)$, where ϕ_c is the percolation threshold for the gelatin/graphene systems. The red line in the inset is the fit to the data based on the power law equation with a correlation factor of 0.9995.

hydrophobic interaction between gelatin and the basal plane of graphene sufficiently strong to prevent graphene from aggregation during the chemical reduction. Therefore, the excellent dispersion of graphene nanosheets can be attributed to this novel preparation method. Scanning electron microscopy (SEM) observations of gelatin/graphene nanocomposite films confirm the above results (Figure 3d). Well-organized layered structures of graphene nanosheets over the cross-section of the film indicate the adsorption of gelatin onto the graphene surfaces without disturbing the two-dimensionality of the nanoobjects.

The electrical conductivity behavior of nanocomposites with different graphene concentration was investigated by the four-point probe method (Kelvin sensing). A rapid increase in the direct electrical conductivity was observed at low volume fraction (**Figure 4**). For conductivity evaluation, it is more convenient to measure the loading of graphene in terms of volume fractions, making use of gelatin and graphene densities (see the Supporting Information). At a loading of 0.11 vol%, the electrical conductivity of this nanocomposite is 8.9×10^{-5} S m^{-1}, which is higher than the antistatic criterion (10^{-6} S m^{-1}) for thin films.[44] An increase in graphene loading above 0.5 vol% yields a more gradual increase in the electrical conductivity, e.g., ≈1 S m^{-1} and 5 S m^{-1} at 2.7 and 5 vol%, respectively. It is worth mentioning that ascorbic acid has no significant effect on the conductivity properties of the samples (Table S2, Supporting Information). This rapid increase in electrical conductivity is usually observed when a conductive filler forms well-defined interconnected paths through the insulating matrix. Conductivity for rigid nanoparticles is typically described with the bond percolation model.[45] Above the percolation threshold, the bond percolation model yields a power law, $\sigma_c = \sigma_f [(\phi - \phi_c)/(1 - \phi_c)]^t$, for the conductivity of the composite, where σ_f is the conductivity of the filler, ϕ the filler volume fraction, ϕ_c the percolation threshold, and t is the so-called "universal critical exponent".[46] In our gelatin–graphene nanocomposites, the percolation occurs when the filler concentration is $\phi_c = 3.3 \times 10^{-2}$ vol% (Figure 4). To the best of our knowledge, this percolation threshold is about two times lower than the lowest values reported for graphene-based nanocomposites,[47] and five times lower than the best value for CPCs;[48] to rationalize this value taking randomly oriented oblate ellipsoids (disks-like objects) as a benchmark,[49] such a percolation threshold would be accessible only through oblates having an aspect ratio of $a/b > 1000$ (Figure S3, Supporting Information), which seems a plausible extreme flatness to mimic the graphene 2D structure. Thus, such a low percolation threshold can be conclusively attributed to the extremely high aspect ratio of the graphene nanosheets and their excellent homogeneous dispersion in the nanocomposites.

The linear fit of the log–log plot of conductivity σ versus $(\phi - \phi_c)/(1 - \phi_c)$ results in values for the critical exponent of $t = 2.53 \pm 0.05$ and for the inherent filler conductivity of $\sigma_f = 10^{3.9 \pm 0.1}$ S cm^{-1}(Figure 4 inset). The exponent t depends on the dimensionality of the conductive network and has a theoretical value of $t = 2$ for 3D networks.[45] However, considerable deviations from $t = 2$ have been reported in the literature. For instance, t values as large as 2.73,[48] 4.18,[50] and 3.47[47] have been reported for various classes of polymer/graphene nanocomposites. Considering tunneling of the charge carriers through the insulating matrix as the main conduction mechanism in graphene-based networks, the obtained t exponent is significantly below 3 in our system, which implies a broad distribution of interparticle separations within the gelatin/graphene nanocomposite.[51,52]

The mechanical properties of the nanocomposites were also examined by quantitative nanomechanical (QNM) AFM (PeakForce QNM) (Figure S4, Supporting Information). Specifically, we measured the out-of-plane moduli of the nanocomposite films which increased from 0.5 ± 0.07 GPa for the pure gelatin film to 3.0 ± 0.7 GPa for the nanocomposite film containing 10 wt% graphene nanosheets (Figure S4, Supporting Information).

The impermeability of graphene films to gases and liquids in general poses severe limits to its application in sensing.[53] Here, however, the intrinsic ability of gelatin to adsorb moisture opens new sensing possibilities in biosensor design.

The humidity sensing properties of gelatin/graphene nanocomposite films were investigated at different relative humidity (RH) values at room temperature. The linear I–V curves for the gelatin/graphene nanocomposite film indicate good ohmic contact between the composite film and the electrodes. In addition, under a sweeping voltage, the current decreases and then increases upon increasing RH (**Figure 5**a). The electrical conductivity of the film was evaluated from the slope of the I–V curve, and the results shown in Figure 5b exhibit a correlation between the electrical conductivity and RH. First, a decay in the electrical conductivity of the nanocomposite upon increasing the RH from 0% to 70% was observed, which is related to the swelling of the gelatin network and the consequent increase of the graphene nanosheets distance, i.e., decrease in the number of contacts. Second, an increase in the electrical conductivity beyond RH values of 70% can be attributed to the ionic conductivity of charged species whose mobility is enhanced by the high level of free water (high water activity, a_w) in the nanocomposite.[54,55] Therefore, the humidity-sensing mechanism of the

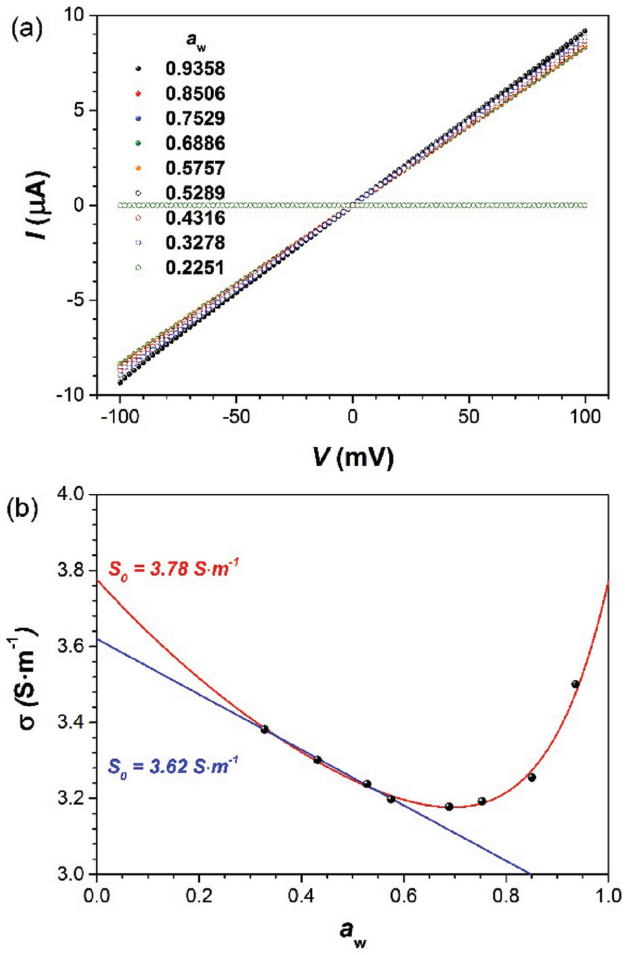

Figure 5. Humidity-sensing properties of gelatin/graphene nanocomposite films. a) *I–V* plot characteristic of the gelatin/graphene nanocomposite at various RH levels with sweeping voltage (–100 to 100 mV). b) The conductivity of the gelatin/graphene nanocomposite as a function of RH (filler concentration in nanocomposite is 10 wt%).

gelatin/graphene nanocomposite films switches from electrical conductivity at low and medium RH values to ionic conductivity at higher water activities. If the range of water activity is known ($a_w < 0.7$ or $a_w > 0.7$), the nanocomposites can be used as a sensor in the full relative-humidity range; if not, use can be made only in any of the two branches of monotonic behavior. Thus, these gelatin/graphene nanocomposite films can be seen as promising systems for highly sensitive humidity sensors, also considering the good stability of the nanocomposite films in aqueous media (see Figure S5, Supporting Information).

In summary, we have presented a novel method for the preparation of bio-inspired, waterborne, and biocompatible conductive biopolymer nanocomposites with very well-dispersed graphene nanoparticles within the gelatin matrix. The electrical properties of these nanocomposites are comparable to the best values reported in the literature,[46,48,50,56] yet with a percolation threshold lower than the lowest values ever reported for graphene nanocomposites (0.06 vol%),[47] and for conductive biopolymer nanocomposites (0.15 vol%).[48] This unprecedented low threshold could open new opportunities in the search of optically transparent electrodes, for example. Additionally, due to the water adsorption features of gelatin matrices, the corresponding graphene nanocomposites can be used in applications such as biosensors and stimuli-responsive systems triggered by RH variations.

Supporting Information

Supporting Information is available from the Wiley Online Library or from the author.

Acknowledgements

The authors thank ETH Zurich/ScopeM for the experimental facilities and Infrastructure. S. Busato and A. Daus are acknowledged for assisting with the electrical conductivity measurements. H.N. kindly acknowledges the Graduate Student Scholarship from the Ministry of Science, Research and Technology of Iran.

Received: February 25, 2016
Revised: April 30, 2016
Published online: June 1, 2016

[1] V. Mittal, *Nanocomposites with Biodegradable Polymers*, Oxford University Press, New York **2011**.
[2] X. Wang, H. Bai, Z. Yao, A. Liu, G. Shi, *J. Mater. Chem.* **2010**, *20*, 9032.
[3] B. Kumar, M. Castro, J. F. Feller, *Sens. Actuators, B* **2012**, *161*, 621.
[4] Y. Feng, X. Zhang, Y. Shen, K. Yoshino, W. Feng, *Carbohydr. Polym.* **2012**, *87*, 644.
[5] D. G. Zarate-Triviño, E. Prokhorov, G. Luna-Bárcenas, J. Mendez-Nonell, J. B. González-Campos, E. Elizalde-Peña, J. D. Mota-Morales, P. Santiago-Jacinto, M. Terrones, S. Gómez-Salazar, S. M. Nuño-Donlucas, I. C. Sanchez, *Mater. Chem. Phys.* **2015**, *155*, 252.
[6] P. Musto, P. Russo, F. Cimino, D. Acierno, G. Lupò, C. Petrarca, *Eur. Polym. J.* **2015**, *64*, 170.
[7] H. Fan, L. Wang, K. Zhao, N. Li, Z. Shi, Z. Ge, Z. Jin, *Biomacromolecules* **2010**, *11*, 2345.
[8] C. Li, J. Adamcik, R. Mezzenga, *Nat. Nanotechnol.* **2012**, *7*, 421.
[9] G. Boran, *Gelatin: Production, Applications and Health Implications*, Nova Science Publishers Inc., New York, **2013**.
[10] H. Vanveelen, G. F. Borginion, *J. Photogr. Sci.* **1969**, *17*, 81.
[11] D. Baziwane, Q. He, *Food Rev. Int.* **2003**, *19*, 423.
[12] V. Rattanaruengsrikul, N. Pimpha, P. Supaphol, *Macromol. Biosci.* **2009**, *9*, 1004.
[13] Y. Lee, J. W. Bae, J. W. Lee, W. Suh, K. D. Park, *J. Mater. Chem. B* **2014**, *2*, 7712.
[14] A. A. Dongargaonkar, G. L. Bowlin, H. Yang, *Biomacromolecules* **2013**, *14*, 4038.
[15] I. S. Raja, N. N. Fathima, *Colloids Surf., B* **2015**, *128*, 537.
[16] F. J. Martínez-Vázquez, M. V. Cabañas, J. L. Paris, D. Lozano, M. Vallet-Regí, *Acta Biomater.* **2015**, *15*, 200.
[17] W. Li, H. Wang, Y. Ding, E. C. Scheithauer, O.-M. Goudouri, A. Grünewald, R. Detsch, S. Agarwal, A. R. Boccaccini, *J. Mater. Chem. B* **2015**, *3*, 3367.
[18] Y. Marois, N. Chakfé, X. Deng, M. Marois, T. How, M. W. King, R. Guidoin, *Biomaterials* **1995**, *16*, 1131.
[19] P. Laaksonen, A. Walther, J. Malho, M. Kainlauri, O. Ikkala, M. B. Linder, *Angew. Chem., Int. Ed.* **2011**, *50*, 8688.

[20] T. H. Han, W. J. Lee, D. H. Lee, J. E. Kim, E.-Y. Choi, S. O. Kim, *Adv. Mater.* **2010**, *22*, 2060.
[21] P. Laaksonen, M. Kainlauri, T. Laaksonen, A. Shchepetov, H. Jiang, J. Ahopelto, M. B. B. Linder, *Angew. Chem., Int. Ed.* **2010**, *49*, 4946.
[22] A. J. Patil, J. L. Vickery, T. B. Scott, S. Mann, *Adv. Mater.* **2009**, *21*, 3159.
[23] C. Wan, M. Frydrych, B. Chen, *Soft Matter* **2011**, *7*, 6159.
[24] C. Cha, S. R. Shin, X. Gao, N. Annabi, M. R. Dokmeci, X. Tang, A. Khademhosseini, *Small* **2014**, *10*, 514.
[25] S. R. Shin, B. Aghaei-Ghareh-Bolagh, T. T. Dang, S. N. Topkaya, X. Gao, S. Y. Yang, S. M. Jung, J. H. Oh, M. R. Dokmeci, X. S. Tang, A. Khademhosseini, *Adv. Mater.* **2013**, *25*, 6385.
[26] Y. Piao, B. Chen, *J. Polym. Sci., Part B: Polym. Phys.* **2015**, *53*, 356.
[27] K. Liu, J.-J. Zhang, F.-F. Cheng, T.-T. Zheng, C. Wang, J.-J. Zhu, *J. Mater. Chem.* **2011**, *21*, 12034.
[28] Y. Ge, J. Wang, Z. Shi, J. Yin, *J. Mater. Chem.* **2012**, *22*, 17619.
[29] Y. Piao, B. Chen, *RSC Adv.* **2016**, *6*, 6171.
[30] W. Wang, Z. Wang, Y. Liu, N. Li, W. Wang, J. Gao, *Mater. Res. Bull.* **2012**, *47*, 2245.
[31] M. Lian, J. Fan, Z. Shi, S. Zhang, H. Li, J. Yin, *Carbon* **2015**, *89*, 279.
[32] M. J. Fernández-Merino, L. Guardia, J. I. Paredes, S. Villar-Rodil, P. Solís-Fernández, A. Martínez-Alonso, J. M. D. Tascón, *J. Phys. Chem. C* **2010**, *114*, 6426.
[33] J. Zhang, H. Yang, G. Shen, P. Cheng, J. Zhang, S. Guo, *Chem. Commun.* **2010**, *46*, 1112.
[34] I. Childres, L. A. Jauregui, W. Park, H. Cao, Y. P. Chen, E. S. G. Doyle, in *Development in Photon and Materials Research*, Nova Science Publishers, New York **2013**, pp. 978–981.
[35] A. C. Ferrari, D. M. Basko, *Nat. Nanotechnol.* **2013**, *8*, 235.
[36] H. Wang, J. T. Robinson, X. Li, H. Dai, *J. Am. Chem. Soc.* **2009**, *131*, 9910.
[37] H. Wang, Y. Wang, X. Cao, M. Feng, G. Lan, *J. Raman Spectrosc.* **2009**, *40*, 1791.
[38] A. C. Ferrari, J. C. Meyer, V. Scardaci, C. Casiraghi, M. Lazzeri, F. Mauri, S. Piscanec, D. Jiang, K. S. Novoselov, S. Roth, A. K. Geim, *Phys. Rev. Lett.* **2006**, *97*, 187401.
[39] H. Kim, C. W. Macosko, *Macromolecules* **2008**, *41*, 3317.
[40] Q. Li, Z. Li, M. Chen, Y. Fang, *Nano Lett.* **2009**, *9*, 2129.
[41] M. Hirata, T. Gotou, S. Horiuchi, M. Fujiwara, M. Ohba, *Carbon* **2004**, *42*, 2929.
[42] H. Kim, Y. Miura, C. W. Macosko, *Chem. Mater.* **2010**, *22*, 3441.
[43] L. E. R. O'Leary, J. A. Fallas, E. L. Bakota, M. K. Kang, J. D. Hartgerink, *Nat. Chem.* **2011**, *3*, 821.
[44] D. D. L. Chung, *J. Mater. Sci.* **2004**, *39*, 2645.
[45] D. Stauffer, A. Aharony, *Introduction to Percolation Theory*, Taylor & Francis, London, UK **2003**.
[46] S. Stankovich, D. A. Dikin, G. H. B. Dommett, K. M. Kohlhaas, E. J. Zimney, E. A. Stach, R. D. Piner, S. T. Nguyen, R. S. Ruoff, *Nature* **2006**, *442*, 282.
[47] N. H. Vo, T. D. Dao, H. M. Jeong, *Macromol. Chem. Phys.* **2015**, *216*, 770.
[48] Z. Tang, H. Kang, Z. Shen, B. Guo, L. Zhang, D. Jia, *Macromolecules* **2012**, *45*, 3444.
[49] E. J. Garboczi, K. A. Snyder, J. F. Douglas, M. F. Thorpe, *Phys. Rev. E* **1995**, *52*, 819.
[50] M. Yoonessi, J. R. Gaier, *ACS Nano* **2010**, *4*, 7211.
[51] R. Zhang, M. Baxendale, T. Peijs, *Phys. Rev. B* **2007**, *76*, 195433.
[52] C. Grimaldi, I. Balberg, *Phys. Rev. Lett.* **2006**, *96*, 66602.
[53] R. R. Nair, H. A. Wu, P. N. Jayaram, I. V Grigorieva, A. K. Geim, *Science* **2012**, *335*, 442.
[54] M. Khan, S. Schuster, M. Zharnikov, *J. Phys. Chem. C* **2015**, *119*, 14427.
[55] W.-D. Lin, C.-T. Liao, T.-C. Chang, S.-H. Chen, R.-J. Wu, *Sens. Actuator B Chem.* **2015**, *209*, 555.
[56] C. Gao, S. Zhang, F. Wang, B. Wen, C. Han, Y. Ding, M. Yang, *ACS Appl. Mater. Interfaces* **2014**, *6*, 12252.